THE EFFECTS OF LEADING AND TRAILING EDGE DETAILS ON THE FLOW AROUND ELONGATED BLUFF BODIES

Emanuela Palombi, Gregory A. Kopp, Roi Gurka
Boundary Layer Wind Tunnel Laboratory
Faculty of Engineering, University of Western Ontario
London, Ontario, N6A 5B9, Canada
gak@blwtl.uwo.ca

ABSTRACT

The influence of leading and trailing edge geometry on the flows around four elongated cylinders was examined. In particular, the mean flow characteristics around the bodies (including the distance from the leading edge to the reattachment point, the boundary layers thickness at the the trailing edge, the speed-up at the leeward trailing edge) and in the wakes, particularly the details of the vortex streets, were examined. It was found that there is no simple scaling relationship linking the various vortex street parameters such as the spacing ratio, *b/a*, the vortex convection speeds, and vortex strengths so that there is no universal Strouhal number for these flows. It appears that the diffuse separated shear layers are the main cause of this lack of universality in vortex streets, so that each vortex street depends on the precise way it came to be formed.

INTRODUCTION

The Storebælt Bridge, Denmark, was the longest suspension bridge in the world when it opened in 1998. About one month before opening, it experienced large amplitude oscillations at a low wind speed, due to vortex shedding (Frandsen, 2001). The amplitudes were of sufficient magnitude and at such a common wind speed that they would eventually cause fatigue problems, as well as lead to significant occupant (driver) comfort issues. This led to an expensive retro-fit; turning vanes were welded onto the lower corners of the deck along the length of the span. This type of problem has been relatively infrequent, but could become more significant as bridge decks become longer and lighter. Geometry is one of the crucial factors that influence the flow characteristics and aeroelastic response of long-span bridges and other elongated bluff bodies. Since the flow field and the vortex shedding activity produced by the wind-structure interaction are complex, the largely unknown effects of deck geometry lead to ad-hoc design solutions.

Relatively few studies have been performed on elongated bluff bodies, where an elongated bluff body is defined as a cross-section with a chord length which is long enough so that there is reattachment on the body following leading edge separations. Okajima (1982) showed that, for rectangular cylinders, the afterbody disrupts the interaction of the two separated shear layers and leads to a suppression of the Kármán-like vortex street. Because of such effects by the leading edge separations and the subsequent reattachments on the boundary layers along the body, it is reasonable that there should be different flow mechanisms and instabilities as the elongation ratio, defined as the chord-to-thickness ratio (*l/h*), is altered. For example, Stokes and Welsh's (1986) study of bodies of rectangular cross-section, found that there are four regimes defined by *l/h*. In particular, they found that the first regime is for $l/h < 3.2$, the body of the cylinder does not disrupt the interaction of the shear layers and a Kármán street exists. However, for an elongation ratio within the second regime ($3.2 < l/h < 7.6$), they observed that there is no Kármán street present and that the shear layers reattach to the body intermittently. As a result, the wake is disorganized in this regime. Also observed with increasing *l/h* is that the Strouhal number, when defined by the chord, follows a stepwise increase with elongation ratio. Recently, Mills et al. (2003) explained that the jumps in the Strouhal number are due to the number of vortices traveling across the body for a given elongation ratio. Following the work of Stokes and Welsh (1986), Nakamura et al. (1991) observed an impinging shear layer instability which arose from the interaction of the reattaching shear layer with the trailing edge. They argued that this created a feedback which alters the vorticity production at the leading edge. However, Mills et al. proposed that the primary instability is an impinging leading edge vortex (ILEV) instability where the vortices formed from the separation at the leading edge travel along the deck interfering with the formation region. In any case, different flow instabilities clearly exist, which depend significantly on the body geometry.

Thus, the objectives of the experimental program are to determine how the leading and trailing edge details, as well as elongation ratio, affect the flow around the body, the flow instabilities the aerodynamic loads, and the relationships between these. The current experiments focus on four different body geometries, all at the same elongation ratio, in order to develop a basic understanding of the effects of the leading and trailing edge details. Since the ultimate application of this work is for long-span bridge design, for each model the leading and trailing edge details are identical.

EXPERIMENTAL SET-UP

Model Details

The experiments were carried out in a 0.45m x 0.45m cross section by 1.5m long test section of an open return wind tunnel at the Boundary Layer Wind Tunnel Laboratory (BLWTL) at the University of Western Ontario. Four smooth, elongated bluff bodies with distinct leading and trailing edge geometries were tested. Each had an

elongation ratio, i.e., chord-to-thickness ratio, of 7. Three of the models were symmetric, having leading and trailing edges of rectangular, triangular and semi-circular shape, as shown in Fig. 1. The cross-section of the fourth model, which is asymmetric about the horizontal axis, resembles the Storebælt Bridge.

Each cylinder was mounted horizontally in the mid-plane of the working section, approximately 0.3m downstream of the inlet. Spanning the full width of the working section and securely fastened to the tunnel glass windows on each side, the aspect ratio of all four models was 18. The thickness of each model was h = 0.025m so that the blockage ratio was 5%. No corrections were made for blockage effects. The coordinate system is aligned with the origin centrally located at the centerline or mid-span of the cylinder, as shown in Fig. 2. The x-axis is set in-line with the direction of the free-stream velocity, U_∞, and the y-axis is found normal to the cylinder axis and to the flow in the lateral direction. The tunnel speed was set at 17.8m/s, yielding a moderately high Reynolds number of $3x10^4$, based on h.

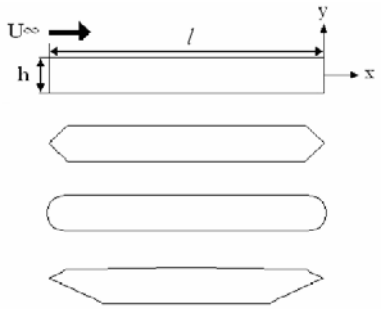

Figure 1: Definition sketch of the Rectangular, Triangular, Circular and Storebælt models.

Pressure Measurements

All four models had a set of 24 pressure taps, aligned in a ring at midspan. The reader is referred to Palombi (2006) for the tap locations on each model. The taps were connected to pressure scanners via a tubing system. The tubing system had a frequency response which was flat to beyond 200 Hz. During the experiments, the pressures were low pass filtered at 200 Hz, then sampled simultaneously at a rate of 400/sec/channel, for 150 seconds. The pressure time histories were integrated to give time histories of the sectional lift, drag and torque.

Particle Image Velocimetry Measurements

A TSI PIV system with a 120 mJ/pulse double Nd:YAG laser was used in this study. Olive oil was used with an in-house Laskin nozzle to seed the flow and a 1024 x 1024 pixel charge-coupled device (CCD) camera was used to capture the wake behavior. The lens fitted to the camera had a focal length range of 60mm and the object distance was adjusted to obtain a field-of-view of approximately 9.5h x 9.5h. The spatial resolution of the images captured, with a 32 x 32 pixel interrogation window and 50% overlapping, was 3.68 mm. The acquired images were analyzed using TSI Insight® software. Standard filters were applied to remove erroneous vectors such as: global and local standard deviation and a median which resulted in about 5% of the vectors. The PIV frames were sampled at approximately 15 Hz and the time delay between image pairs was set within the range of 12-16μs for all experiments. A total of 3000 vectors maps were acquired for each model.

MEAN FLOW CHARACTERISTICS

For vortex shedding phenomena, it is well established that the detailed characteristics of the separated shear layers, and the distance between them are key factors in the formation of vortex streets (Roshko, 1954; Bearman, 1967). Thus, the relevant aspects of the mean flow for elongated bluff bodies are the characteristics of the boundary layers immediately upstream of the leeward flow separations as well as the formation region immediately downstream of the body. In this manuscript, we focus on three aspects; specifically, (i) the distance from the leading edge to the first reattachment, (ii) the boundary layer profiles at the leeward separation point (which is not necessarily the trailing edge for these geometries), and (iii) the length of the recirculation zone in the base region of the wake.

Table 1 indicates the distance of the reattachment point from the leading edge, x_R, as inferred from the pressure measurements. The reattachment length is significantly shorter for the triangular, circular and Storebælt models, when compared to the rectangular cylinder. Reattachment on the rectangular cylinder is downstream of the mid-plane, at approximately 2/3h from the leading edge, while for the triangular cylinder it is at about 1/3h, and for the circular model it is at about 1/7h. The flow around the Storebælt model is more complex with separation at the "nose", the reattachment on the angled surfaces and small subsequent separation bubbles at the edges prior to the surfaces becoming parallel with the upstream flow. As will be discussed further below, the drag coefficients are consistent with x_R; earlier reattachment is associated with lower drag as one would expect from make bodies more streamlined.

Plots of the mean streamwise velocity profiles near the point of separation for all four bodies are found in Figure 2. Due to the asymmetric design of the Storebælt model, profiles for both the upper and lower trailing edges are presented. Note that the origin of the vertical axis is located at the along the centreline, at trailing edge for the symmetric cross-sections (see Figure 1); however for the Storebælt model, the origin of the lateral positioning is fixed at the off-centered height where the upper and lower trailing edge surfaces meet. The PIV data for the rectangular model could not be resolved within a lateral distance of approximately 0.25h from the solid boundary. However, it is clear that the rectangular model has a boundary layer, δ_{TE}, that is thickest at the trailing edge. The triangular, Storebælt (lower followed by upper trailing edge surface) and circular models follow in decreasing order. Table 1 presents δ_{TE} for all four models.

Speed-up ratios, U_δ/U_∞, from the edge of the boundary layer at the leeward separation point can be found in Table 1. Slight speed-ups in mean velocities (excluding the rectangular cylinder) are observed, the values being much smaller than the values observed from other bluff bodies such as circular cylinders or normal flat plates. The most significant speed-ups are apparent at the lower trailing edge flange of the Storebælt model, and the semi-circular model, where increases of approximately 10 and 4.5 percent,

respectively are observed. These small speed-up values imply that any observed vortex streets in the wake will not follow the universal scaling of vortex shedding found by Bearman (1967), a point which will be examined in greater detail below.

Table 1: Mean flow properties around the bodies and in the near wake.

Model	x_R/h	δ_{TE}/h	U_δ/U_∞	θ/h	x_W/h
Rectangular	0.67	1.20	1.00	0.67	1.0
Triangular	0.33	0.76	1.02	0.42	0.33
Circular	0.14	0.42	1.05	0.26	0.66
Storebaelt[1]	0.25	0.37	1.03	0.34	0.12
	0.35	0.48	1.11		

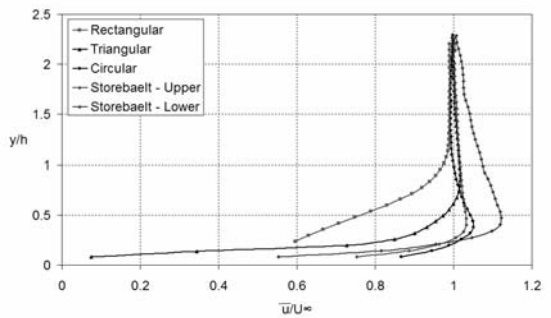

Figure 2: Mean trailing edge streamwise velocity profiles.

A comparison of the mean streamwise velocity profiles measured at $x = 2h$ is shown in Figure 3. It is evident that the rectangular cylinder produces the widest wake at this location, with the triangular cylinder following in size. Interestingly, the circular and Storebælt cylinders seem to exhibit a similar wake width however, the circular model exhibits a smaller velocity defect and so has lower drag.

The mean wake profiles presented can also give insight regarding the recirculation region located directly behind each cylinder. Because there exists a large variation in the streamwise velocities measured at mid-height behind the four cylinders, the formation lengths must be considerably different. Table 1 presents values for the momentum thickness, θ and the length of the recirculation region, x_W. Again, x_W is largest for the rectangular cylinder and the smallest for the Storebælt model.

The sectional pressure drag coefficients of the four models are given in Table 2. The drag coefficient is found to be the highest for the rectangular model, and the triangular model again follows second. Contrary to what is inferred by the similar wake widths of the circular and Storebælt models previously shown in the mean wake velocity profiles in Fig. 3, the drag coefficients found for these cylinders are quite different. It is apparent that the minimal loss of momentum in the mean wake flow in the circular model case causes it to exhibit the least drag force.

Aerodynamic forces, the details of the recirculation zone and vortex shedding are all linked in the literature. It is generally understood that the size of the mean wake recirculation region decreases in the presence of vortex shedding (Balachandar et al., 1997). Trends in the measured Strouhal frequencies, shown in Table 2, can be shown by the formation length theory established by Roshko (1954), i.e., if the scale of the formation region is reduced, the shedding frequency increases. Thus, Roshko argued that streamlining tends to increase the shedding frequency. This is, in part, contingent on the proximity of the shear layers, but the detailed results are not entirely consistent with this, as discussed further in the next section, where details of vortex shedding are examined.

VORTEX SHEDDING

Strouhal Numbers

Measurements of the shedding frequency were made via the peak values observed in the power spectral density functions (PSDF) of the lift fluctuations. These frequencies were non-dimensionalized using the thickness of the model, h, and the free stream velocity, U_∞, so that the Strouhal number is

$$St = \frac{f_s h}{U_\infty} \tag{1}$$

The frequencies and resulting Strouhal numbers are presented in Table 2. The Storebælt model was found to have the highest frequency measured at 198 Hz and has a spectral peak which is narrowband peak, while the lowest frequency is the rectangular model at 105 Hz. The rectangular model has the weakest peak, which is also quite broadband. The triangular and semi-circular models also have strong, narrowband peaks. Examination of the fluctuating drag shows that the rectangular cylinder has no peak frequencies, while the other three models exhibit the same narrowband peaks as for the lift fluctuations. This type of spectral activity for the rectangular cylinder resembles the observations in Parker and Welsh (1983), for similar experimental parameters. In particular, they observed no sharp spectral peaks in the wakes of rectangular plates with elongation ratios greater than 7.6, at a Reynolds number of approximately $5\text{x}10^4$.

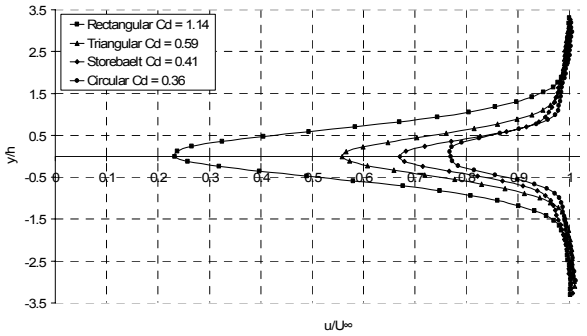

Figure 3: Mean streamwise velocities at $x/h = 2$.

Ensemble-Averages of the Vortex Street

In order to quantify the frequency-centred activity in the wakes we use a vortex identification technique of Jeong and Hussain (1995). This vortex identification scheme defines a vortex core in incompressible flow in terms of the eigenvalues of the symmetric tensor $S^2 + \Omega^2$: where S and Ω

[1] Because of the asymmetry in the Storebaelt model, where two numbers are present, these refer to the upper and lower surfaces or shear layers, as appropriate.

are the symmetric and anti-symmetric parts of ∇u . In two-dimensions, this method is identical to examining the invariants of the velocity gradient tensor as is done in critical point theory. Like all methods, this one is also sensitive to the presence of mean shear. Nevertheless, in vortex street wakes where one would assume that all of the mean shear is caused by the passing vortices, this is an effective method.

Table 2: Aerodynamic and vortex shedding parameters determined from surface pressure measurements.

Model	C_D	C_L'	f_s	St
Rectangular	1.14	0.037	106	0.15
Triangular	0.59	0.055	133	0.19
Circular	0.36	0.046	164	0.24
Storebaelt	0.41	0.030	198	0.28

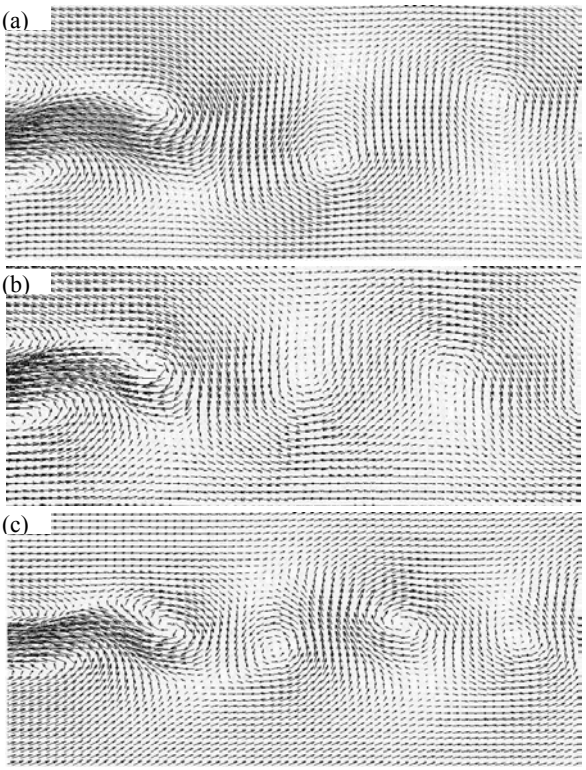

Figure 4: Ensemble-averages of vortices aligned at $x/h = 2$ for the (a) triangular, (b) circular and (c) Storebælt models. Flow is from left to right and the convection speed is $U_c = 0.85U_\infty$ in order to view the vortices further downstream.

Once the vortex cores were identified, individual patterns were ensemble-averaged based on location of the vortex centers. In this case, vortices at $x = 2h$ downstream of the trailing edge were aligned and averaged. The results for the triangular, semi-circular and Storebaelt models are shown in Figure 4. It can be observed that these wakes have Kármán-like vortex streets which account for the frequency content in the lift and drag spectra. The ensemble-averaged fields will be analyzed in greater detail below.

No coherent vortices could be obtained with the vortex identification technique for the rectangular cylinder due to the relative disorder in this wake. Undoubtedly, there are vortices, as shown by the vorticity contours in Figure 5; however, the flow instability appears to be completely different with respect to the other models.

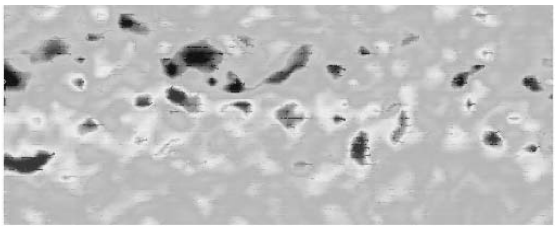

Figure 5: Vorticity contours in a single PIV frame for the rectangular cylinder.

Vortex Convection Speeds

The streamwise velocity measured at the center of the ensemble-averaged vortex is defined as the vortex convection speed, U_c. The observed convection speeds found for each case vary considerably at $x = 2h$, as shown in Table 3. The triangular model has the slowest convective speed of approximately $0.68U_\infty$, while the Storebælt model has the fastest at approximately $0.75U_\infty$. So, the variation is about 10% at this location in the flow.

The convection speeds of the vortices are not constant as they travel downstream. It was found that at $x = 6h$, the ensemble averaged vortices for all three flows had similar convection speeds, being in a range near 84-85% of the free-stream velocity. Note that Figure 4 illustrates the ensemble-averaged flow field with this convection speed removed from the vectors. It may be that the different formation locations in the flows all lead to the difference in U_c at $x = 2h$. Additionally, potential flow theory indicates that the spacing ratio of the vortices, b/a, is closely related to the vortex convection speeds (e.g., Bearman, 1967), and all three have different spacing ratios, as will be shown below. On the other hand, the boundary layers at the trailing edge all have different profiles, some with local speed-ups, as indicated in Figure 1 and Table 1. Interestingly, the ratio, $U_c/U_\delta \sim 0.7$, is nearly constant for these three flows[2]. Since, by $x = 6h$, the convection speeds are nearly constant, this does not seem to play a major role in the wake dynamics, in contrast to what is implied by the potential flow analysis.

Table 3: Ensemble-averaged properties of the vortex streets.

Model	U_c/U_∞	b/a	ΔA	$\Gamma_o /U_\infty h$	Γ/Γ_o
Rectangular	n/a	n/a	n/a	n/a	n/a
Triangular	0.68	0.39	1.31	7.48	0.44
Circular	0.73	0.29	0.76	5.36	0.58
Storebaelt	0.75	0.17	0.84	6.70	0.61
			1	4.32	0.38

Vortex Street Spacing Ratio

The classical description of a vortex street was first quantified by von Kármán. His specific anti-symmetric structure, exhibiting neutral stability, was characterized with a spacing ratio, $b/a = 0.281$, where b is the lateral distance between vortex rows and a is the inter-vortex spacing in one row. Experimentally, this spacing ratio has not been

[2] For the Storebaelt model, we have used the average value.

justified, with various authors have observed differing b/a ratios ranging from 0.16 to 0.40. Figure 4 clearly shows that the spacing ratio is altered in the three flows examined, while this is quantified in Table 3.

The street spacing ratios are consistent with the wake thickness and drag results presented for the three bodies. A connection to the proximity of the separated shear layers in each case can be made. The distance between the separated shears layers produced by the circular and Storebælt models appear to be comparable and are consistent with the mean wake profiles. The triangular model not only produces the widest wake of the three, it is found that the rows of vortices tend to diverge.

Examining the St and b/a ratios indicates that the vertical spacing of the vortices is not related to the horizontal spacing in a simple way. Roshko (1954) introduced the concept of the universal Strouhal number, St_u, where the distance between the separated shear layers replaces the body thickness and the speed at the separation point replaces the free stream speed. There are several ways this can be analyzed for elongated bluff bodies. If one presumes that the all of the effects of the leading edge details are contained within the mean velocity profile at the separation point, then the distance between the separated shear layers could be represented by ($2\delta_{TE} + h$), and the speed by U_δ, so that

$$St_u = \frac{f_s(2\delta_{TE} + h)}{U_\delta} \tag{2a}$$

In contrast, one could also relate the vortex street parameters directly into a universal Strouhal number if one replaces the shedding frequency, f_s, as U_c/a, the separation between the shear layers with b, and the separation speed with U_δ, so that,

$$St_u = \frac{U_c}{U_\infty}\frac{U_\infty}{U_\delta}\frac{b}{a} \tag{2b}$$

(Bearman, 1967). These parameters are presented in Table 4. Clearly, Equation 2(b) overcompensates for the variation in the Strouhal frequency so that the variation is actually greater than the Strouhal number indicated by Equation (1). This is due primarily to the very significant changes in the spacing ratio, b/a, with the flow details. In contrast, using the Equation 2(a), which are upstream (of the wake) parameters are a better parameter, but there is still significant variation (about 20% between the largest and smallest values), outside of experimental uncertainties.

Table 4: Universal Strouhal numbers.

Model	$\frac{f_s(2\delta_{TE}+h)}{U_\delta}$	$\frac{U_c}{U_\infty}\frac{U_\infty}{U_\delta}\frac{b}{a}$
Triangular	0.46	0.26
Circular	0.40	0.20
Storebaelt	0.48	0.12

Vortex Circulation Strength and Size

The circulation in a vortex can be estimated as:

$$\Gamma(x) = \sum_{i,j}\langle\omega\rangle_{i,j}\Delta A_{i,j} \tag{3}$$

where ω is the vorticity and ΔA is the vortex area. The vortex area was found by plotting the circulation strength against the area of the vortex measured 2h downstream of the trailing edge, in the ensemble-averaged wake of each cylinder. The center of the ensemble-averaged vortex, where the maximum vorticity is found, was chosen as the starting point for the numerical integration. As the area of the integration was increased, it was observed that the circulation would reach a plateau, consistent with theoretical expectations. So, at the point that the integration became constant, the area of the vortices was obtained. These values have significant uncertainty and because of this, emphasis is placed on the relative magnitudes of the vortices for each case. Table 3 presents the relative vortex size, ΔA, and circulations, Γ, normalized by values obtained for the lower row from the Storebælt model (which were observed to be weakest).

The vortices shed from the triangular model were found to be the largest and strongest vortices, causing the wake width to be the widest of the three models. The circular model produced the smallest vortices; however, these were not the weakest. A difference of the size was found amongst the vortices shed from the upper and lower shear layers for the Storebælt model. In this case, the vortices in the top row are relatively smaller then those in the bottom – but still not as small as those shed by the circular edge model. The asymmetry in the model plays a significant role since the vortices in the upper and lower rows are of different strengths. It is peculiar to note that the size of the vortices shed at the lower corner are larger those of shed at the upper corner, but are found to be weaker in strength. It is believed that because the circulation is measured at $x = 2h$ downstream of the trailing edge, the lower shear layer travels a longer distance from the initial point of separation. This leads to weaker vortices, consistent with the effects of asymmetry observed in other flows by Bailey et al. (2002).

In an attempt to link the strength of the vortex street produced by the three shedding bodies and the fluctuating lift, Table 2 also contains the RMS lift coefficient values, C_L', found for each model. The triangular model sheds the strongest vortices and is consequently subjected to the largest fluctuating forces. In the case of the Storebælt model, the vortices shed from the upper shear layer are approximately 1.5 times stronger then those of the lower surface; in this case, the lift fluctuations are shown to be the least of the three models.

To further investigate the differences between the three vortex streets, and the geometries that cause them, the effect of available circulation at the trailing edge needs to be examined. Adjacent to the upper and lower surfaces of the body, the shear layers are considered to be thin and are characterized as two-dimensional vortex sheets. Saffman (1992) defined the circulation of a vortex sheet, Γ_o, as:

$$\Gamma_o = \int \sigma ds \approx \sigma L \tag{4}$$

where, σ is the vortex sheet strength and s is the spatial coordinate in the direction along the trailing edge streamline. Following the analysis of Bailey et al. (2002), the length, L, is the length from separation to the end of the mean recirculation region. The vortex sheet strength is found as an integral of the vorticity across the vortex sheet, and the vorticity is defined as

$$\omega = -\frac{\partial q}{\partial n} + K_s q \tag{5}$$

where, q is the magnitude of the velocity, n is the spatial coordinate in the direction normal to the trailing edge streamline and K_s is the curvature of the streamline (Bailey et al., 2002). K_s was found by plotting the mean trailing edge flow fields for all four cylinders and extracting a streamline which initiated at $y = \delta$ above the point of separation on the trailing edge, then extended to the end of the mean recirculation region in the near wake. Therefore, the final expression of the vortex sheet strength is provided in terms of the velocity differential across the vortex sheet,

$$\sigma = -\partial q + \int_{u=0}^{\delta} K_s q dn \qquad (6)$$

Assuming that the streamwise component of the flow within the direct vicinity of the upper and lower surfaces of the body is approximately zero, the total circulation available at the trailing edge is contingent on the magnitude of the velocity at the outer limit of the existing trailing edge boundary layer, the magnitude of the trailing edge streamline curvature and the vortex sheet length via the integral in Equation (4). Bailey et al. (2002) argue that the shear layer strength can be effectively increased if one or all of the following variables are increased: (i) the velocity gradient across the sheet (ii) the curvature along the shear layer streamline and (iii) the length of the shear layer extending into the near wake. The trailing edge circulation, Γ_o, also provides insight as to the amount of circulation that is captured by the coherent structures in the wake and how much is lost to the surrounding turbulence. In Table 3 the ratios, Γ/Γ_o, are presented in terms of the available circulation at the trailing edge and the circulation strength of the vortices measured at $x = 2h$, for each model. All cylinders seem to follow the observations made by many authors, which indicate that approximately 50% of the available circulation is entrained to the shed vortices, although there is significant variation in the results.

In light of the scaling of a universal Strouhal number, the circulations in the wake vortices and available at the trailing edge are interesting. Clearly, the longer the distance from separation point to the end of the recirculation region in the wake, the lower the proportion of vorticity the ends up in the wake vortices. The lower row of the Storebaelt model has particularly low proportion of 38% because of the long distance from the seaparation at the lower flange while the triangular model has a low value as well, consistent with the long recirculation length in that flow. Over such a length, significant diffusion of the separated shear layer occurs, so that the vortices are relatively weaker.

Bearman's (1967) splitter plate experiments show that more diffuse shear layers lead to changes in the vortex spacing ratio, much like the increased *b/a* observed for the triangular model. Thus, if appears that diffused shear layers is the main cause of the lack of a universal Strouhal number for the present elongated bluff bodies.

CONCLUSIONS

The flow fields around four models of elongation ratio of 7 and Re = 30,000 were examined. The rectangular cylinder did not have a periodic vortex street, but did have coherent lift fluctuations at a Strouhal number, *St = 0.15*. The three remaining models did produce vortex streets which were observed to be quite sensitive to the body geometry. Analysis indicated that the typical characteristics of vortex streets including spacing ratios, *b/a*, vortex convection speeds, U_c/U_∞, speed-up factors at the separation point, U_δ/U_∞, had complex relationships such that no universal Strouhal number could be found for these shapes. This is believed to be caused by the level of diffuseness in the separated shear layers, such that each vortex street depends of the detailed path to formation and there is a lack of universality in vortex street wakes.

ACKNOWLEDGEMENTS

This work was partially supported by the National Science and Engineering Research Council of Canada. Equipment was purchased through support from the Canada Foundation for Innovation, the Ontario Research and Development Challenge Fund and the University of Western Ontario's Academic Development Fund. One of the authors (G.A. Kopp) gratefully acknowledges the support from the Canada Research Chairs Program.

REFERENCES

Bailey, S. C. C., Kopp, G. A. and Martinuzzi, R. J., 2002, "Vortex shedding from a square cylinder near a wall", J. Turbulence, 3, 1.

Balachandar, S., Mittal, R. and Najjar, F. M., 1997, "Properties of the mean recirculation region in the wakes of two-dimensional bluff bodies", J. Fluid Mech., 351, 167.

Bearman, P. W., 1967, "On vortex street wakes", J. Fluid Mech., 28, 625.

Frandsen, J. B., 2001, "Simultaneous pressures and accelerations measured full-scale on the Great Belt East Suspension Bridge", J. Wind. Eng. Ind. Aerodyn., 89, 95.

Jeong, J. and Hussain, F., 1995, "On the Identification of a Vortex", J. Fluid Mech., 285, 69.

Mills, R., Sheridan, J., and Hourigan, K., 2003, "Particle image velocimetry and visualization of natural and forced flow around rectangular cylinders", J. Fluid Mech., 478, 299.

Nakamura, Y., Ohya, Y., and Tsuruta, H., 1991, "Experiments on vortex shedding from flat plates with square leading and trailing edges", J. Fluid Mech., 222, 437.

Okajima, A., 1982, "Strouhal numbers of rectangular cylinders", J. Fluid Mech., 123, 379.

Palombi, E., 2006, "Effects of geometry on the flow around elongated cylinders", M.E.Sc. thesis, University of Western Ontario, London, Canada.

Parker, R. and Welsh, M. C., 1983, "Effects of Sound on Flow Separation from Blunt Flat Plates", Intl J. Heat Fluid Flow Eng., 4, 113.

Roshko, A., 1954, "On the drag and shedding frequency of two-dimensional bluff bodies", National Advisory Committee for Aeronautics, NACA Technical Note 3169.

Saffman, P.G., 1992, "Vortex dynamics", Cambridge University Press, Cambridge.

Stokes, A.N. and Welsh, M.C., 1986, "Flow-resonant sound interaction in a duct containing a plate. Part II: Square leading edge", J. Sound Vib., 104, 55.